Interaction and Multiscale Mechanics, Vol. 3, No. 2 (2010) 111-121
DOI: http://dx.doi.org/10.12989/imm.2010.3.2.111

Atomistic analysis of nano/micro biosensors

James Chen and James D. Lee*

Department of Mechanical and Aerospace Engineering, The George Washington University, Washington DC 20052, USA

(Received January 7, 2010, Accepted May 10, 2010)

Abstract. Dynamic analysis of nano/micro bio-sensors based on a multiscale atomistic/continuum theory is introduced. We use a generalized atomistic finite element method (GAFEM) to analyze a bio-sensor which has $3 \times N_a \times N_p$ degrees of freedom, where N_p is the number of representative unit cells and N_a is the number of atoms per unit cell. The stiffness matrix is derived from interatomic potential between pairs of atoms. This work contains two studies: (1) the resonance analysis of nano bio-sensors with different amount of target analyte and (2) the dependence of resonance frequency on finite element mesh. We also examine the Courant-Friedrichs-Lewy (CFL) condition based on the highest resonance frequency. The CFL condition is the criterion for the time step used in the dynamic analysis by GAFEM. Our studies can be utilized to predict the performance of micro/nano bio-sensors from atomistic perspective.

Keywords: atomistic field theory; nanosensor; resonance frequency; courant condition.

1. Introduction

Microcantilevers were first designed and fabricated for use as force sensors. Possessing an extremely high force sensitivity, in the piconewton (pN) range, the cantilevers have made Atomic Force Microscopy (AFM) (Binnig *et al*. 1986) universally recognized not only as a versatile microscopy technique with high spatial resolution but also as a powerful tool for measuring the forces between surfaces. Nowadays cantilevers have been further used as biosensors since Clark and Lyons in 1962 made an amperometric sensor detecting glucose level in blood (Fritz 2008).

When the size of micro/nano cantilever bio-sensors is getting smaller and down to nano scale, the classical beam theory (Finot *et al.* 2008) and classical finite element formulation (Sheeparamatti *et al*. 2006) are not accurate enough to describe the static/dynamic behavior. On the other hand, molecular dynamics (MD) simulation provides high accuracy but expensive computational cost. As a compromise, in this work, we adopt Atomistic Field Theory developed by Chen and Lee (2005, 2006) to resolve this dilemma. It is an atom-embedded continuum theory which integrates concurrently atoms and continua. It has the accuracy of molecular dynamics but is less expensive. Lee *et.al.* formulate a generalized atomistic finite element method (GAFEM) to numerically implement this field theory for systems at micro/nano scale (Lee and Chen 2008).

The outline of this paper is arranged as follows: in Section 2, the resonance analyses are discussed

* Corresponding author, Professor, E-mail: jdlee@gwu.edu

in beam theory, classical finite element method, generalized atomistic finite element method (GAFEM), and MD simulation. In Section 3, three different problems are discussed. The first one is the shift of the resonance frequency due to different amount of target analyte. The second one is the effect of finite element mesh size on the first resonance frequency. The third one is a short discussion on the Courant-Friedrichs-Lewy condition in GAFEM. This paper ends with a brief summary and discussion.

2. Resonace analysis in different theories

2.1 Beam Theory

Cantilevers bend when loading is applied. The whole system is simulated as an ideal spring-mass system. The spring constant k is the proportionality factor between applied force f and the resulting bending displacement x. It is widely known as Hooke's Law.

$$f = kx \tag{1}$$

For cantilever beam, the spring constant can be expressed as

$$k = \frac{Ewb^3}{4L^3} \tag{2}$$

where E is Young's modulus, w is the cantilever width, b is the thickness and L is the length. Then the resonance frequency is obtained as

$$\omega = \sqrt{\frac{k}{m^*}} \tag{3}$$

where m^* is an effective mass (taking into account the cantilever geometry and mass distribution along the cantilever). It is noticed that only one resonance frequency is computed in using beam theory. Its application is very limited due to lots of closure hypotheses in the beam theory and specified beam shape assumption.

2.2 Classical finite element method (Classical continuum)

In this method, continuum is discretized into elements and nodes. Assume that the stress tensor is a function of strain tensor only and there is no damping. The governing equation becomes

$$\boldsymbol{M}\ddot{\boldsymbol{U}} + \boldsymbol{K}\boldsymbol{U} = \boldsymbol{f} \tag{4}$$

where $\boldsymbol{M}$ is the mass matrix, $\boldsymbol{K}$ is the stiffness matrix, $\boldsymbol{U}$ is the displacement vector, and $\boldsymbol{f}$ is the vector of applied force. The resonance frequencies of the system can be obtained through the eigenvalue analysis

$$\det(\boldsymbol{K} - \omega^2\boldsymbol{M}) = 0 \tag{5}$$

where ω is a set of resonance frequencies. If there is no constraint on an N-node system, $3N$ resonance frequencies can be found. Above micro size, this approach is very useful and accurate.

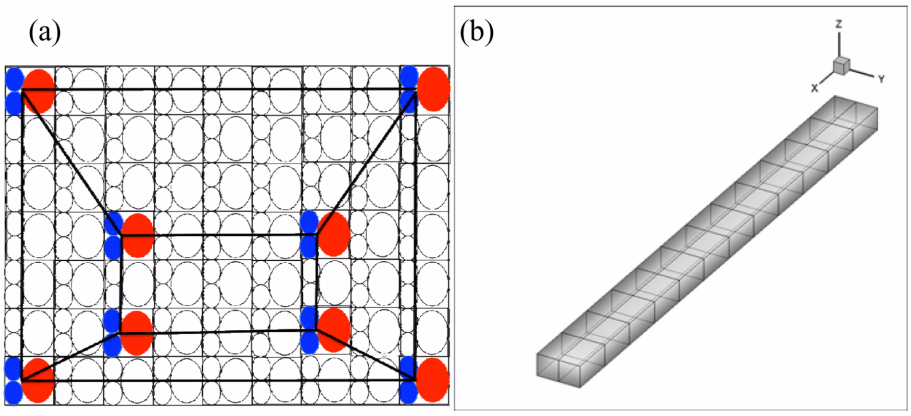

Fig. 1(a) Schematic diagram of single crystal, including crystal lattices, finite element meshes and nodes, (b) GAFEM mesh for cantilever sensor

2.3 Generalized atomistic finite element method (Atom-embedded continuum)

Crystalline solids are distinguished from other states of matter by a periodic arrangement of the atoms; such a structure is called a Bravais lattice. Essentially, the regularity displayed by a crystal lattice is that of a three-dimensional mesh which divides space into identical parallelepipeds. Imagine that a number of atoms, referred to as a unit cell, are placed at the intersections of such a mesh; then we have a grain or a single crystal as shown in Fig. 1(a). The distinct feature of this Atomistic Field Theory is that a single crystal is modeled as a continuum in which a point represents a unit cell consisting of a specified number of different atoms, not just an idealized mathematical identity. Therefore a multi-grain material system is considered as a concurrent atomistic/continuum material system. All single crystals (grains) are modeled by this multiscale theory, a continuum theory, but not just a classical continuum theory in which a point only has three degrees of freedom.

In this field theory, the motion could be expressed as

$$\boldsymbol{u}(k,\alpha) = \boldsymbol{r}(k,\alpha) - \boldsymbol{R}(k,\alpha) = \boldsymbol{u}(k) + \boldsymbol{\xi}(k,\alpha) \tag{6}$$

where k and α indicates the α-th atom in the k-th unit cell, $\boldsymbol{u}(k)$ is the displacement of the centroid of the k-th unit cell and $\boldsymbol{\xi}(k,\alpha)$ is the relative displacement of the α-th atom to the centroid. All the physical quantities, including density, displacement, etc., could be expressed in physical and phase spaces and these two spaces are connected through the Dirac delta function and the Kronecker delta function as

$$\boldsymbol{A}(\boldsymbol{x},\boldsymbol{y}^{\alpha},t) = \sum_{k=1}^{N_l}\sum_{\xi=1}^{N_a} a[\boldsymbol{r}(t),\boldsymbol{p}(t)]\,\delta(\boldsymbol{R}^{k}-\boldsymbol{x})\tilde{\delta}(\Delta\boldsymbol{r}^{k\xi}-\boldsymbol{y}^{\alpha}) \tag{7}$$

where $a[\boldsymbol{r}(t),\boldsymbol{p}(t)]$ is any physical quantity in phase space, $\boldsymbol{A}(\boldsymbol{x},\boldsymbol{y}^{\alpha},t)$ is the corresponding density function in physical space, N_a is number of atoms in a unit cell, N_l is number of unit cells, $\delta(\boldsymbol{R}^{k}-\boldsymbol{x})$ is Dirac delta function and $\tilde{\delta}(\Delta\boldsymbol{r}^{k\xi}-\boldsymbol{y}^{\alpha})$ is Kronecker delta function.

From Eqs. (6) and (7), one can find the balance law of linear momentum (Lee and Chen 2008)

$$\boldsymbol{\rho}^{\lambda}\boldsymbol{V}^{*}\ddot{\boldsymbol{u}}^{\lambda} = \nabla_{x}\cdot\boldsymbol{t}^{\lambda}+\boldsymbol{f}^{\lambda}+\boldsymbol{\varphi}^{\lambda} \tag{8}$$

where the kinetic part of stress tensor $\boldsymbol{t}^{\lambda}$ is related to temperature as $t_{ij}^{\lambda} = -\gamma^{\lambda}k_{B}\boldsymbol{T}\boldsymbol{\delta}_{ij}$; $\gamma^{\lambda} = m^{\lambda}/M$; m^{α} is the mass of α-th atom; $M = \sum_{\alpha=1}^{N_a} m^{\alpha}$ is the total mass of a unit cell; $\boldsymbol{V}^{*}$ is the volume of the unit cell; $\boldsymbol{\rho}^{\lambda}$ is the mass density; $\boldsymbol{u}^{\lambda}$ is the displacement of λ-th atom; $\boldsymbol{f}^{\lambda}$ is all the interatomic force acting on λ-th atom; $\boldsymbol{\varphi}^{\lambda}$ is all the body force due to external field acting on the λ-th atom.

This work is a special case in which T=0. Then Eq. (8) can be re-written as

$$m^{\lambda}\ddot{\boldsymbol{u}}(k,\lambda) = \boldsymbol{f}(k,\lambda)+\boldsymbol{\varphi}(k,\lambda) \tag{9}$$

where $\boldsymbol{f}(k,\lambda)$ is all the interatomic force acting on λ-th atom in the k-th unit cell; $\boldsymbol{\varphi}(k,\lambda)$ is all the body force due to external field acting on the λ-th atom in the k-th unit cell.

In this work, we restrict our attention to pair potential which can be expanded in Taylor Series as

$$\begin{aligned} V^{ij}(|\boldsymbol{r}^{i}-\boldsymbol{r}^{j}|) &= V^{ij}(r^{ij}) \\ &= V^{ij}(R^{ij})+\sum_{\lambda}\left.\frac{\partial V^{ij}(r^{ij})}{\partial \boldsymbol{r}^{\lambda}}\right|_{r^{ij}=R^{ij}}\cdot\boldsymbol{u}^{\lambda}+\frac{1}{2}\sum_{\lambda}\sum_{\mu}\boldsymbol{u}^{\lambda}\cdot\left.\frac{\partial^{2}V^{ij}(r^{ij})}{\partial \boldsymbol{r}^{\lambda}\partial \boldsymbol{r}^{\mu}}\right|_{r^{ij}=R^{ij}}\cdot\boldsymbol{u}^{\mu}+\ldots \\ &= V^{ij}(R^{ij})-\sum_{\lambda}\boldsymbol{f}^{\lambda}(R^{ij})\cdot\boldsymbol{u}^{\lambda}+\frac{1}{2}\sum_{\lambda}\sum_{\mu}\boldsymbol{u}^{\lambda}\cdot\boldsymbol{K}^{\lambda\mu}(R^{ij})\cdot\boldsymbol{u}^{\mu}+\ldots \end{aligned} \tag{10}$$

It is noticed that $i\neq j$ and

$$\begin{aligned} \boldsymbol{K}^{\lambda\mu} &= \frac{\partial}{\partial \boldsymbol{r}^{\lambda}}\left(\frac{\partial V^{ij}}{\partial \boldsymbol{r}^{\mu}}\right) \\ &= \frac{\partial}{\partial \boldsymbol{r}^{\lambda}}\left[\frac{\partial V^{ij}}{\partial r^{ij}}\frac{\boldsymbol{r}^{ij}}{r^{ij}}(\boldsymbol{\delta}_{i\mu}-\boldsymbol{\delta}_{j\mu})\right] \\ &= \left(\frac{\partial}{\partial \boldsymbol{r}^{\lambda}}\left(\frac{\partial V^{ij}}{\partial r^{ij}}\frac{1}{r^{ij}}\right)\right)\boldsymbol{r}^{ij}(\boldsymbol{\delta}_{i\mu}-\boldsymbol{\delta}_{j\mu})+\left(\frac{\partial \boldsymbol{r}^{ij}}{\partial \boldsymbol{r}^{\lambda}}\right)\frac{\partial V^{ij}}{\partial r^{ij}}\frac{1}{r^{ij}}(\boldsymbol{\delta}_{i\mu}-\boldsymbol{\delta}_{j\mu}) \\ &= \left\{\left(\frac{\partial}{\partial r^{ij}}\left(\frac{1}{r^{ij}}\frac{\partial V^{ij}}{\partial r^{ij}}\right)\right)\frac{\boldsymbol{r}^{ij}\otimes\boldsymbol{r}^{ij}}{r^{ij}}+\frac{\boldsymbol{I}}{r^{ij}}\frac{\partial V^{ij}}{\partial r^{ij}}\right\}(\boldsymbol{\delta}_{i\lambda}-\boldsymbol{\delta}_{j\lambda})(\boldsymbol{\delta}_{i\mu}-\boldsymbol{\delta}_{j\mu}) \end{aligned} \tag{11}$$

$$\boldsymbol{f}^{\lambda}(R^{ij}) = -\left.\frac{\partial V^{ij}(r^{ij})}{\partial \boldsymbol{r}^{\lambda}}\right|_{r^{ij}=R^{ij}} = -\frac{\partial V^{ij}}{\partial r^{ij}}\frac{\partial r^{ij}}{\partial \boldsymbol{r}^{\lambda}} = -\frac{\partial V^{ij}}{\partial r^{ij}}\frac{\boldsymbol{r}^{ij}}{r^{ij}}(\boldsymbol{\delta}_{i\lambda}-\boldsymbol{\delta}_{j\lambda}) \tag{12}$$

where $\boldsymbol{u}^{\lambda} = \boldsymbol{r}^{\lambda} - \boldsymbol{R}^{\lambda}$ is the displacement of λ-th atom; $\boldsymbol{r}^{\lambda}$ is the current position of λ-th atom; $\boldsymbol{R}^{\lambda}$ is the original position of λ-th atom; $\boldsymbol{I}_{3\times 3}$ is an identity matrix.

$$(\delta_{i\lambda} - \delta_{j\lambda})(\delta_{i\mu} - \delta_{j\mu}) = \begin{cases} 1, & \text{if } \lambda = \mu = i \text{ or } \lambda = \mu = j \\ -1, & \text{if } (\lambda = i \text{ and } \mu = j) \text{ or } (\lambda = j \text{ and } \mu = i) \\ 0, & \text{otherwise} \end{cases} \tag{13}$$

For example, let the interatomic potential be the Coulomb-Buckingham potential

$$V^{ij} = \frac{q^i q^j}{r^{ij}} + A^{ij} e^{-\frac{r^{ij}}{B^{ij}}} - C^{ij}(r^{ij})^{-6} \tag{14}$$

where q^i is electric charge of i-th atom; r^{ij} is the interatomic distance between i-th and j-th atoms; A^{ij}, B^{ij} and C^{ij} are material constants. The stiffness matrix can be derived as

$$\begin{aligned} \boldsymbol{K}^{\lambda\mu} &= \left\{ \frac{\boldsymbol{I}}{r^{ij}} \frac{\partial V^{ij}}{\partial r^{ij}} + \left(\frac{\partial}{\partial r^{ij}} \left(\frac{1}{r^{ij}} \frac{\partial V^{ij}}{\partial r^{ij}} \right) \right) \frac{\boldsymbol{r}^{ij} \otimes \boldsymbol{r}^{ij}}{r^{ij}} \right\} \Bigg|_{r^{ij} = R^{ij}} (\delta_{i\lambda} - \delta_{j\lambda})(\delta_{i\mu} - \delta_{j\mu}) \\ &= (M\boldsymbol{I} + N\boldsymbol{r}^{ij} \otimes \boldsymbol{r}^{ij})\big|_{r^{ij} = R^{ij}} (\delta_{i\lambda} - \delta_{j\lambda})(\delta_{i\mu} - \delta_{j\mu}) \\ &= \tilde{\boldsymbol{K}}\big|_{r^{ij} = R^{ij}} (\delta_{i\lambda} - \delta_{j\lambda})(\delta_{i\mu} - \delta_{j\mu}) \end{aligned} \tag{15}$$

where

$$\begin{aligned} M &= \frac{1}{r^{ij}} \frac{\partial V^{ij}}{\partial r^{ij}} = \frac{q^i q^j}{(r^{ij})^3} + \frac{A^{ij}}{B^{ij} r^{ij}} e^{-\frac{r^{ij}}{B^{ij}}} - \frac{6C^{ij}}{(r^{ij})^8} \\ N &= \frac{\partial M}{\partial r^{ij}} \frac{1}{r^{ij}} = -3\frac{q^i q^j}{(r^{ij})^5} - \frac{A^{ij}}{B^{ij}(r^{ij})^2} e^{-\frac{r^{ij}}{B^{ij}}} \left(\frac{1}{r^{ij}} + \frac{1}{B^{ij}} \right) + \frac{48C^{ij}}{(r^{ij})^{10}} \end{aligned} \tag{16}$$

The two-atom stiffness matrix, $\boldsymbol{K}^*$, is obtained as

$$\boldsymbol{K}^* = \begin{bmatrix} \boldsymbol{K}^{\lambda\lambda} & \boldsymbol{K}^{\lambda\mu} \\ \boldsymbol{K}^{\mu\lambda} & \boldsymbol{K}^{\mu\mu} \end{bmatrix} = \begin{bmatrix} \tilde{\boldsymbol{K}} & -\tilde{\boldsymbol{K}} \\ -\tilde{\boldsymbol{K}} & \tilde{\boldsymbol{K}} \end{bmatrix} \tag{17}$$

From Eqs. (9) and (10), we may rewrite Eq. (9) as

$$m^{\alpha} \ddot{\boldsymbol{u}}^{k\alpha} + \sum_{l} \sum_{\beta} \boldsymbol{K}^{k\alpha l\beta} \boldsymbol{u}^{l\beta} = \sum_{l} \sum_{\beta} \boldsymbol{f}^{k\alpha l\beta}(R^{k\alpha l\beta}) + \boldsymbol{\varphi}^{k\alpha} \tag{18}$$

where k refers to the k-th unit cell; α refers to the α-th atom in k-th unit cell; $\boldsymbol{K}^{k\alpha l\beta}$ is the stiffness

matrix in Eq. (17) with λ indicating $k\alpha$-th atom and μ indicating $l\beta$-th atom. Let the specimen be decomposed into 8-node solid finite elements. Through shape functions, the displacement field can be linked to the corresponding nodal values as

$$\boldsymbol{u}^{k\alpha} = \sum_{I=1}^{8} N_I(k)\,\boldsymbol{U}^{\alpha}_{I_p(I,k)} \tag{19}$$

where $N_I(k)$ is the I-th shape function of which the value depends on the location of the k-th unit cell; $I_p(I,k)$ is the node number corresponding to the I-th Gauss point of the element where the k-th unit cell resides.

Now we write Eq. (18) as

$$\sum_k \left\{ m^{\alpha}\ddot{\boldsymbol{u}}^{k\alpha} + \sum_l \sum_\beta \boldsymbol{K}^{k\alpha l\beta}\boldsymbol{u}^{l\beta} - \sum_l \sum_\beta \boldsymbol{f}^{k\alpha l\beta}(R^{k\alpha l\beta}) - \boldsymbol{\varphi}^{k\alpha} \right\} \delta\boldsymbol{u}^{k\alpha} = 0 \tag{20}$$

Substituting Eq. (19) into Eq. (20), it results

$$\sum_{J=1}^{8} \sum_k N_J(k) \left\{ \sum_{I=1}^{8} m^{\alpha} N_I(k)\,\ddot{\boldsymbol{U}}^{\alpha}_{I_p(I,k)} + \sum_l \sum_\beta \sum_{I=1}^{8} N_I(l)\boldsymbol{K}^{k\alpha l\beta} \cdot \boldsymbol{U}^{\beta}_{I_p(I,l)} - \sum_l \sum_\beta \boldsymbol{f}^{k\alpha l\beta}(R^{k\alpha l\beta}) - \boldsymbol{\varphi}^{k\alpha} \right\} \delta\boldsymbol{U}^{\alpha}_{I_p(J,k)} = 0 \tag{21}$$

Since Eq. (21) must be valid for any arbitrary virtual displacement $\delta\boldsymbol{U}^{\alpha}_{I_p}$, it leads to

$$\sum_k \left\{ \sum_{I=1}^{8} m^{\alpha} N_J(k) N_I(k)\,\ddot{\boldsymbol{U}}^{\alpha}_{I_p(I,k)} + \sum_l \sum_\beta \sum_{I=1}^{8} N_I(l) N_J(k) \boldsymbol{K}^{k\alpha l\beta} \cdot \boldsymbol{U}^{\beta}_{I_p(I,l)} - \sum_l \sum_\beta N_J(k)\boldsymbol{f}^{k\alpha l\beta}(R^{k\alpha l\beta}) - N_J(k)\boldsymbol{\varphi}^{k\alpha} \right\} = 0 \tag{22}$$

Eq. (22) can be properly assembled into a more compact form

$$\boldsymbol{M}\ddot{\boldsymbol{U}} + \boldsymbol{K}\boldsymbol{U} = \boldsymbol{F} + \boldsymbol{\varphi} \tag{23}$$

From the mass matrix and the stiffness matrix, one can calculate the natural frequencies of the system through eigenvalue analysis. If the system is discretized into N_p nodes and each node is a representative unit cell with N_a atoms, the number of natural frequencies is $3 \times N_a \times N_p$. It is seen that this theory integrates atoms into continuum. It provides the accuracy of MD simulation but does not need expensive computation.

2.4 Molecular dynamics simulation

When the element size of GAFEM reduces to lattice constant, the governing equation of the system is exactly the same as that in molecular dynamics. If the number of lattices is N_l, the number of resonance frequencies will be $3 \times N_l \times N_a$.

Table 1 Interatomic potential coefficients of MgO

	Coulomb-Buckingham potential		
	Mg-Mg	Mg-O	O-O
A (eV)	0	929.62	9547.96
B ($\AA^{-1}$)	0	0.29909	0.21916
C ($eV\,\AA^{-6}$)	0	0	32.32

Table 2 Interatomic potential coefficients of $BaTiO_3$

	Coulomb-Buckingham potential		
	Ba-O	Ti-O	O-O
A (eV)	4818.416	4545.823	9547.96
B ($\AA^{-1}$)	0.03067	0.261	0.21916
C ($eV\,\AA^{-6}$)	0	0	32.32

3. Computation examples

The material used in the work is barium titanate ($Ba^{2+}Ti^{4+}O_3^{2-}$) and magnesia ($Mg^{2+}O^{2-}$). The interatomic potential parameters are listed in Table 1 and Table 2 (Chen *et al.* 2010). Barium titanate has five atoms in a unit cell: one barium, one titanium, and three oxygen. It has a lattice constant 7.54567634 Bohr (1 Bohr = $5.291772108 \times 10^{-11}$ m). Magnesia has 8 atoms in a conventional unit cell: four magnesium and four oxygen. It has a lattice constant, 7.93684912 Bohr. The cut-off radius is 22.6767 Bohr for all cases.

3.1 Resonance analysis of nano cantilever sensor

The material used in this case is barium titanate and is 240 lattices in length, 20 lattices in width and 10 lattices in thickness. The mesh is shown in Fig. 1(b). On the surface, it is assumed that 40 gold atoms are uniformly spread as adhesive layer for receptors. The total target hybridized DNA mass is $5 \times 10^9\ m_e$ (electron rest mass, $5 \times 10^9\ m_e \approx 4.5547 \times 10^{-21}\ kg$), which is roughly equivalent to 152 30-bp double stranded DNA. Before coating gold atoms, the first fundamental frequency is 22.916 *KHz*. After coating gold without any hybridization, the frequency shifts to 22.900 *KHz*. Two different distributions of hybridization are studied. The first one assumes that the distribution is always uniform. The second one assumes the hybridization is randomly distributed based on hybridization percentage. In other words, if 40% of total target mass is attached, 40% of the whole surface is randomly covered. The mass randomly distributed on the same node more than once is prohibited. In Fig. 2, the numerical results show that these two cases are very similar. It implies the hybridization distribution does not affect the dynamic performance of micro/nano bio/chemical sensor.

Notice that the weight of maximum possible target analyte is much less than that of the nano cantilever, *i.e.*, $m << M$. The natural frequency is linearly shifted and can be derived as follows.

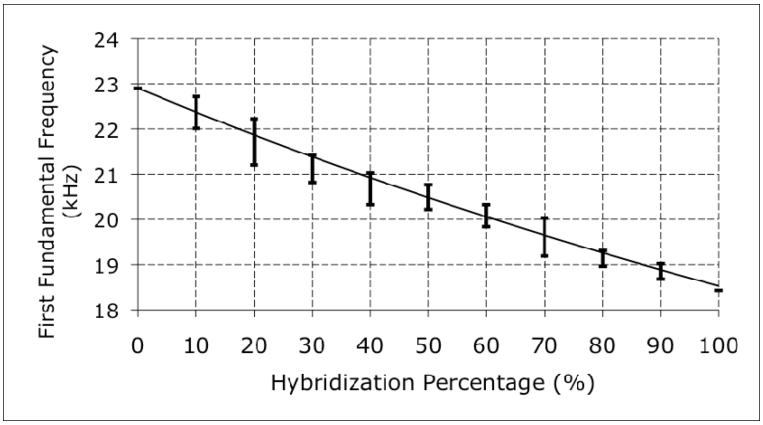

Fig. 2 The shift of the first fundamental frequency. The dashed line with error bar is the result of random distribution and the error bar is the standard deviation of 10 different distributions; the solid line is the result of uniform distribution

$$\omega^* = \sqrt{\frac{K}{M^*}} = \sqrt{\frac{K}{(M+m)}} \approx \sqrt{\frac{K}{M(1+m/M+(m/2M)^2)}} \qquad (\because\ m << M)$$
$$= \sqrt{\frac{K}{M}}\frac{1}{(1+m/2M)} = \omega\frac{1}{(1+m/2M)} \Rightarrow \omega \approx \omega^*(1+m/2M) \qquad (24)$$

where m is additional mass of attached target analyte and M is the mass of the nano/micro cantilever sensor. In Fig. 2, one can notice that even when the target DNA concentration is relatively low, the sensitivity of the sensor is still significant (4 kHz for 4.5547×10^{-3} femto-gram).

3.2 Mesh dependence tests

Here we test two specimens made of barium titanate. Both specimens have 2 lattice constants in width (y-direction) and 1 lattice constant in thickness (z-direction). Respectively, the lengths (x-direction) are 24 lattice constants and 120 lattice constants for the first and second specimens. The number of finite elements in y-direction and z-direction are respectively 2 and 1. Fig. 3 (specimen 1) shows the relation between the first resonance frequency and the number of finite elements in the x-direction. It is observed the first resonance frequency is approaching a constant value as the finite element size approaching the lattice constant. This constant value is the same as one would observe from MD simulation. If the number of finite elements is small, then the finite element model tends to be stiffer than the one with more elements. In other words, the model with less number of elements makes the specimen artificially and mistakenly stiff. It explains why the first resonance frequency drops to instead of rising to the constant value. In Fig. 4, the first fundamental frequency converges to another constant value. Comparison between the two cases, it is seen that the finite element size which converges to the constant value is around one tenth of the specimen length. It means for specimen 1 (24 lattices), the element size needs to be at most 3 lattice constants, and for specimen 2 (120 lattices), the element size needs to be at most 12 lattice constants. It also can be interpreted as 10 nodes are good enough to express the first mode shape.

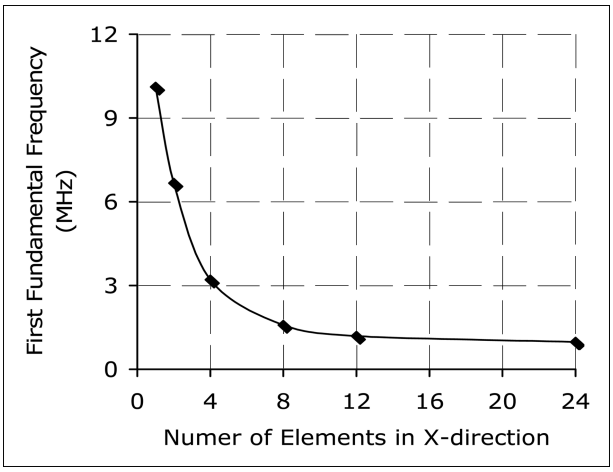

Fig. 3 Mesh dependence Test I for the 24-lattice specimen

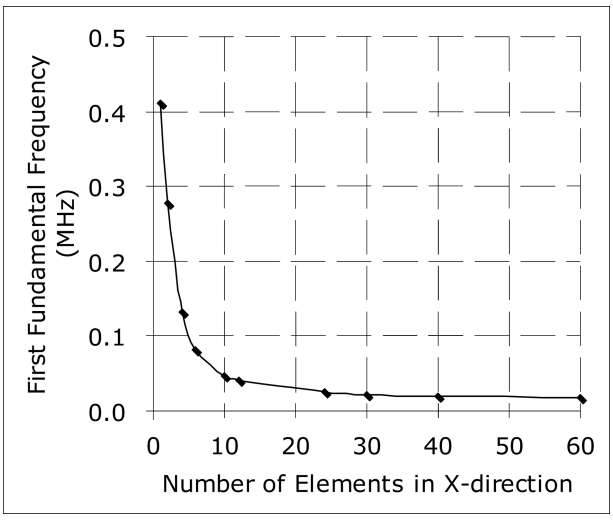

Fig. 4 Mesh dependence Test II for the 120-lattice specimen

3.3 Courant-Friedrichs-Lewy condition

The Courant-Friedrichs-Lewy condition (CFL condition) provides a criterion for the maximum time step in solving hyperbolic-type PDE numerically. The original concept from Courant *et al.* is derived from the eigenvalue analysis (Courant *et al.* 1967), specifically

$$\Delta t \le \Delta t_{critical} \equiv \frac{2}{\omega_{max}} \tag{25}$$

where ω_{max} is the largest natural frequency of this linear system.

In the classical finite element method, the time needed for the wave traveling across the smallest element is equal to $\Delta t_{critical}$ in the CFL condition. That means, for 1-D case

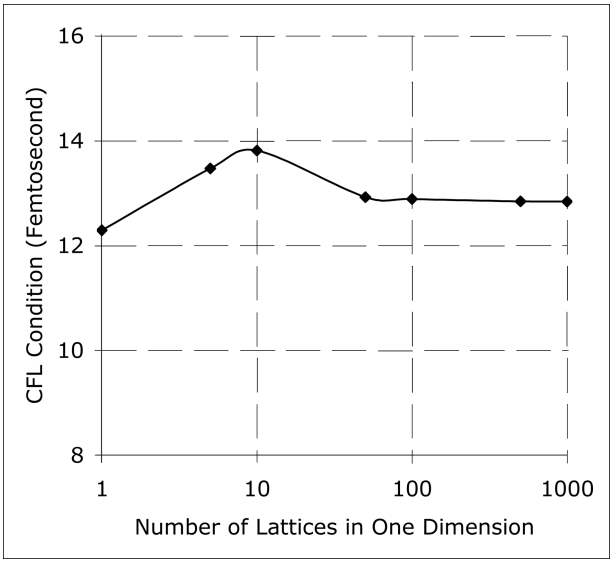

Fig. 5 CFL condition (Time Step) vs. specimen size in one element

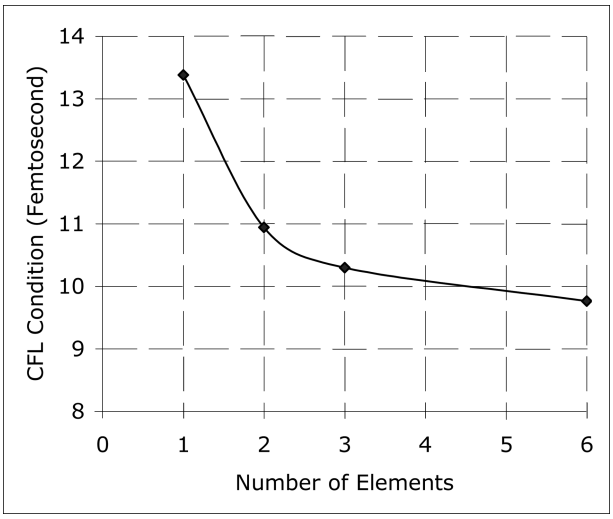

Fig. 6 CFL condition (Time Step) vs. number of finite elements (in one dimension). The specimen size is fixed to 6 lattice constants (in one dimension).

$$\Delta t \leq \Delta t_{critical} = \frac{\Delta x}{u} \tag{26}$$

where u is the wave propagation speed; Δt is the time step; Δx is the smallest element size.

However since GAFEM is based on a nonlocal interatomic potential, $\Delta t_{critical}$ depends on ω_{max}; in other words, the number of elements, not the element size, determines the CFL condition. In GAFEM, the CFL condition based on wave propagation is not valid due to the nonlocal effect.

In this case, we used magnesia (MgO) to demonstrate the CFL condition. Fig. 5 shows that the maximum time step, $\Delta t_{critical}$, is almost a constant due to the nonlocal effect, especially when the number of lattices is sufficiently large. In this case the specimen size changes from 1 lattice to 1000 lattices (in one dimension) but all in one finite element. Fig. 6 shows when the number of elements increases, the maximum resonance frequency becomes larger and hence the required time step is getting smaller. In this case, the specimen size is fixed as $6 \times 6 \times 6$ lattices but the number of elements ranges from 1 to 6 in all directions.

To compare with the noise of cantilever, the first eigenmode of the thermal noise of a micro-sized cantilever sensor at room temperature is around 10,290 Hz (Rast *et al*. 2000). In other words, the micro-sized cantilever oscillates once in every 9.7×10^{-5} sec. The maximum time step for numerical convergence from the CFL condition is around 10 femto-seconds.

4. Conclusions

In this work, resonance analyses in different theories are discussed. In beam theory, only one approximated resonance frequency is obtained. Once the system is modeled by classical finite element method, *3N* resonance frequencies are obtained (*N* is the number of nodes). Molecular dynamics gives $3 \times N_l \times N_a$ exact resonance frequencies but the computational cost is too expensive. Nevertheless Atomistic Field Theory (AFT) with GAFEM provides a highly accurate solution with inexpensive computational cost. It could be used to precisely predict the dynamic performance of nano/micro bio/chemical sensors, namely the first fundamental resonance frequency.

In micro/nano system, classical continuum mechanics is not valid. We need to resort to Atomistic Field Theory (AFT) and Generalized Atomistic Finite Element Method (GAFEM), of which the mesh dependence and the stability condition have been addressed.

References

Binnig, G., Quate, C.F. and Gerber, C. (1986), "Atomic force microscope", *Phys. Rev. Lett.*, **56**(9), 930-933.

Chen, J., Wang, X., Wang, H., and Lee, J.D. (2010), "Multiscale modeling of dynamic crack propagation", *Eng. Fract. Mech.*, **77**, 736-743.

Chen, Y. and Lee, J.D. (2006), "Conservation laws at nano/micro scales", *J. Mech. Mater. Struct.*, **1**(4), 681-704.

Chen, Y. and Lee, J.D.(2005), "Atomistic formulation of a multiscale field theory for nano/micro solids", *Philos. Mag.*, **85**(33-35), 4095-4126.

Courant, R., Friedrichs, K. and Lewy, H. (1967), "On the partial differential equations of mathematical physics", *IBM J.*, March, 215-234.

Finot, E., Passian, A. and Thundat, T. (2008), "Measurement of mechanical properties of cantilever shaped materials", *Sensors*, **8**, 3497-3541.

Fritz, J. (2008), "Cantilever biosensors", *Analyst*, **133**, 855-863.

Lee, J.D. and Chen, Y. (2008), "Modeling and simulation of a single crystal based on a multiscale field theory", *Theor. Appl. Fract. Mec.*, **50**, 243-247.

Rast, S., Wattinger, C., Gysin, U. and Meyer, E. (2000), "The noise of cantilevers", *Nanotechnology*, **11**, 169-172.

Sheeparamatti, B.G, Hebba M.S., Sheeparamatti, R.B., Math, V.B. and Kadadevaramath, J.S. (2006), "Simulation of biosensors using FEM", *J. Physics: conference Series*, **34**, 241-246.